Efficient photo-induced dielectrophoretic particle trapping on Fe:$LiNbO_3$ for arbitrary two dimensional patterning

Juan F. Muñoz-Martínez,[1,2] Iris Elvira,[1] Mariano Jubera,[1] Angel García-Cabañes,[1,*] José Bruno Ramiro,[2] Cándido Arregui[2] and Mercedes Carrascosa[1]

[1]*Departamento de Física de Materiales, Universidad Autónoma de Madrid, Madrid 28049, Spain*
[2]*Departamento de Mecánica de Fluidos y Propulsión Aeroespacial, Universidad Politécnica de Madrid, Madrid 28040, Spain*
[*]*angel.garcia@uam.es*

Abstract: 1D and 2D patterning of uncharged micro- and nanoparticles via dielectrophoretic forces on photovoltaic *z*-cut Fe:$LiNbO_3$ have been investigated for the first time. The technique has been successfully applied with dielectric micro-particles of $CaCO_3$ (diameter d = 1-3 μm) and metal nanoparticles of Al (d = 70 nm). At difference with previous experiments in *x*- and *y*-cut, the obtained patterns locally reproduce the light distribution with high fidelity. A simple model is provided to analyse the trapping process. The results show the remarkably good capabilities of this geometry for high quality 2D light-induced dielectrophoretic patterning overcoming the important limitations presented by previous configurations.

References and links

1. D. A. Grier, "A revolution in optical manipulation," Nature **424**(6950), 810–816 (2003).
2. P. Y. Chiou, A. T. Ohta, and M. C. Wu, "Massively parallel manipulation of single cells and microparticles using optical images," Nature **436**(7049), 370–372 (2005).
3. O. M. Maragò, P. H. Jones, P. G. Gucciardi, G. Volpe, and A. C. Ferrari, "Optical trapping and manipulation of nanostructures," Nat. Nanotechnol. **8**(11), 807–819 (2013).
4. H. A. Eggert, F. Y. Kuhnert, K. Buse, J. R. Adleman, and D. Psaltis, "Trapping of dielectric particles with light-induced space-charge fields," Appl. Phys. Lett. **90**(24), 241909 (2007).
5. X. Zhang, J. Wang, B. Tang, X. Tan, R. A. Rupp, L. Pan, Y. Kong, Q. Sun, and J. Xu, "Optical trapping and manipulation of metallic micro/nanoparticles via photorefractive crystals," Opt. Express **17**(12), 9981–9988 (2009).
6. M. Esseling, F. Holtmann, M. Woerdemann, and C. Denz, "Two-dimensional dielectrophoretic particle trapping in a hybrid crystal/PDMS-system," Opt. Express **18**(16), 17404–17411 (2010).
7. A. M. Glass, D. von der Linde, and T. J. Negran, "High-voltage bulk photovoltaic effect and the photorefractive process in $LiNbO_3$," Appl. Phys. Lett. **25**(4), 233–235 (1974).
8. B. I. Sturmann and V. M. Fridkin, *Photovoltaic and Photorefractive Effects in Noncentrosymetric Materials* (Gordon & Breach, 1992).
9. E. M. de Miguel, J. Limeres, M. Carrascosa, and L. Arizmendi, "Nonlinear generation of higher-order combinational gratings during sequential recording in $LiNbO_3$," J. Opt. Soc. Am. B **17**, 1440–1446 (2000).
10. M. Esseling, A. Zaltron, N. Argiolas, G. Nava, J. Imbrock, I. Cristiani, C. Sada, and C. Denz, "Highly reduced iron-doped lithium niobate for optoelectronic tweezers," Appl. Phys. B **113**(2), 191–197 (2013).
11. T. B. Jones, *Electromechanics of particles* (Cambridge University Press, 1995).
12. J. Villarroel, H. Burgos, Á. García-Cabañes, M. Carrascosa, A. Blázquez-Castro, and F. Agulló-López, "Photovoltaic versus optical tweezers," Opt. Express **19**(24), 24320–24330 (2011).
13. H. Burgos, M. Jubera, J. Villarroel, A. García-Cabañes, F. Agulló-López, and M. Carrascosa, "Role of particle anisotropy and deposition method on the patterning of nano-objects by the photovoltaic effect in $LiNbO_3$," Opt. Mater. **35**(9), 1700–1705 (2013).
14. S. Glaesener, M. Esseling, and C. Denz, "Multiplexing and switching of virtual electrodes in optoelectronic tweezers based on lithium niobate," Opt. Lett. **37**(18), 3744–3746 (2012).
15. M. Esseling, S. Glasener, F. Volonteri, and C. Denz, "Opto-electric particle manipulation on a bismuth silicon oxide crystal," Appl. Phys. Lett. **100**(16), 161903 (2012).
16. L. Miccio, P. Memmolo, S. Grilli, and P. Ferraro, "All-optical microfluidic chips for reconfigurable dielectrophoretic trapping through SLM light induced patterning," Lab Chip **12**(21), 4449–4454 (2012).

17. M. Jubera, A. García-Cabañes, J. Olivares, A. Alcázar, and M. Carrascosa, "Particle trapping and structuring on the surface of $LiNbO_3$:Fe optical waveguides using photovoltaic fields," Opt. Lett. **39**(3), 649–652 (2014).
18. J. Matarrubia, A. Garcia-Cabañes, J. L. Plaza, F. Agullo-Lopez, and M. Carrascosa, "Optimization of particle trapping and patterning via photovoltaic tweezers: role of light modulation and particle size," J. Phys. D Appl. Phys. **47**(26), 265101 (2014).
19. M. Esseling, A. Zaltron, C. Sada, and C. Denz, "Charge sensor and particle trap based on z-cut lithium niobate," Appl. Phys. Lett. **103**(6), 061115 (2013).
20. F. Agulló-López, G. F. Calvo, and M. Carrascosa, "Fundamentals of Photorefractive Phenomena," in *Photorefractive Materials and Applications 1,* P. Günter and J.P. Huignard, Eds. (Springer, 2006), Chap. 1.
21. C. Arregui, J. B. Ramiro, A. Alcázar, A. Méndez, H. Burgos, A. García-Cabañes, and M. Carrascosa, "Optoelectronic tweezers under arbitrary illumination patterns: theoretical simulations and comparison to experiment," Opt. Express **22**(23), 29099–29110 (2014).
22. S. Grilli and P. Ferraro, "Dielectrophoretic trapping of suspended particles by selective pyroelectric effect in lithium niobate crystals," Appl. Phys. Lett. **92**(23), 232902 (2008).
23. K. Buse, "Light-induced charge transport processes in photorefractive crystals I: Models and experimental methods," Appl. Phys. B **64**(3), 273–291 (1997).
24. P. Günter and J. P. Huignard, eds., *Photorefractive Materials and Applications 1, 2, 3* (Springer, 2007).

1. Introduction

Nowadays trapping and manipulation of micro- and nano-objects is a fundamental issue for many applications in nano- and bio-technology [1–3]. In the last years a new technique for particle manipulation, the so called photovoltaic tweezers (or photorefractive tweezers), has been proposed [4–6]. The basis of this technique is the bulk photovoltaic (PV) effect [7,8] that generates high light-induced electric fields in some ferroelectric crystals. These fields can reach values as high as 10^4-10^5 V/cm for Fe doped $LiNbO_3$ [9,10] and depend on the doping level and light exposure. The field extends to the proximity of the crystal surface (evanescent field) and can trap either charged particles via electrophoretic (coulombian) fields or neutral particles via dielectrophoretic (DEP) forces [11]. In this latter case the evanescent PV field polarize neutral particles and attract them to the substrate. The procedure has been studied and developed during the last years [12–18] and now it is definitely established its capability to trap and structure particles on the surface of the ferroelectric material. Moreover, the technique has a number of key advantages such as parallel manipulation on many particles, low intensity operation (at difference with conventional optical tweezers) or reconfiguration capabilities.

However, although the method works very well for 1D particle structuring, 2D patterning has a limited quality [6,13] because particle alignment in directions parallel to the polar axis of the PV material is not possible. Moreover, the particle pattern does not reproduce the light distribution but presents a contouring effect more pronounced in directions normal to the polar axis. All these effects are a consequence of the directional character of the PV effect. It induces charge transport along the polar *c*-axis of the ferroelectric crystal that is parallel to the crystal surfaces in all previous works because they use *x* or *y*-cut substrates. We will call this geometry parallel configuration. To overcome this problem, only a very recent paper [19] proposes to use a different configuration in which the polar axis is normal to substrate faces (*z*-cut). This latter geometry will be called perpendicular configuration along this work. Using this configuration those authors demonstrate high quality 2D particle structuring but only when the particles are charged, i.e., using electrophoretic forces. In fact, the authors expect difficulties to apply the perpendicular configuration to neutral particles by dielectrophoretic forces. It is worthwhile noting that whereas the photovoltaic charge transport and space charge fields in *x*- and *y*-cut configurations have been largely studied in connection with the photorefractive effect (see [20] and references therein) the theoretical analysis of the *z*-cut geometry, necessary to clarify its possible application for PV DEP patterning, is still lacking.

In this work we have investigated the capability of *z*-cut Fe:$LiNbO_3$ substrate to trap and pattern neutral micro and nanoparticles through PV dielectrophoretic forces. A simple theoretical model is presented to provide a first analysis of this new configuration, showing its ability for dielectrophoretic particle trapping. Then a set of 1D and 2D patterning experiments are performed. The method is successfully applied with dielectric micro-particles of $CaCO_3$ (diameter d = 1-3 μm) and metal nanoparticles of Al (d = 70 nm). High quality 2D particle

patterns that accurately reproduce the light patterns are obtained. To evaluate the advantages of the new configuration particle patterns obtained with the same light distribution in *x*- and *z*-cut substrates are compared.

2. Simple theoretical analysis

The bulk PV effect [7,8], basis of the present particle trapping method, consists in a non-symmetrical light-induced excitation of electrons from impurities giving rise to charge transport along the polar axis of the Fe:$LiNbO_3$ crystal. As a consequence, charge redistribution and the corresponding electric field (PV field) are generated. Most previous reported experiments use *x*- or *y*-cut crystals, with the polar axis parallel to the crystal surface (parallel configuration), whereas in this work we investigate the perpendicular configuration with the polar axis normal to the surface. In Fig. 1 we plot a simple scheme to illustrate the bulk charge distribution generated by the PV effect under homogeneous illumination for both parallel, Fig. 1(a), and perpendicular, Fig. 1(b), configurations respectively. It shows that in the parallel configuration the crystal charges migrate to the edges of the illuminated region perpendicular to the *c*-axis whereas in the perpendicular geometry locate in both surfaces along the whole illuminated region. Note that from simple symmetry arguments, it can be inferred that the orientation of the polar axis should induce anisotropy for surface particle trapping only in the parallel configuration. This suggests that the perpendicular configuration can be advantageous for 2D patterning.

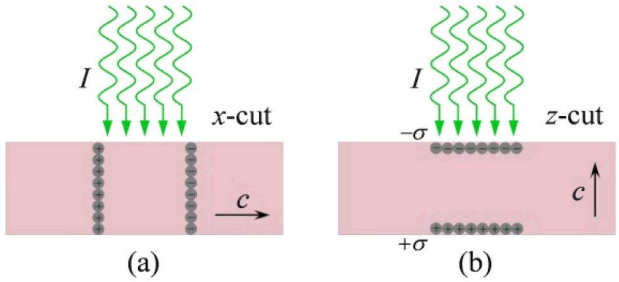

Fig. 1. Schematics of (a) the parallel and (b) perpendicular configurations showing the light induced charge separation due to the photovoltaic effect.

As previously mentioned, a detailed theoretical description for the PV space charge fields and DEP forces developed in *z*-cut has not been addressed so far. In fact, a rigorous theoretical description for the involved perpendicular configuration, including edge effects and non-linear transport (necessary to describe particle trapping), is far from a simple theory. However, it is worthwhile addressing a simple preliminary analysis on the capabilities of the perpendicular configuration for PV DEP particle trapping in order to highlight the main physics involved. To this end, we consider the usual band transport model with one photorefractive center, in our case Fe^{3+}/Fe^{2+}, (see refs [8,20]. for more details). We assume a sinusoidal light illumination $I(x) = I_0(1 + m\cos kx)$, the most commonly used in previous experiments, illuminating the substrate. Due to the photovoltaic effect, an electronic current density $\boldsymbol{j}_{PV}$ establishes along the polar axis (*z* + direction)

$$\boldsymbol{j}_{PV} = esDl_{PV}I\boldsymbol{u}_z \qquad (1)$$

s being the photoinization cross section of donors, *D* the donor concentration ($[Fe^{2+}]$) and l_{PV} the PV drift length (~1-5 Å). This current density leads to charge accumulation and so, to a surface charge density $\sigma(t)$, in both crystal faces (normal to the polar axis) with opposite signs. Any transversal component of the PV charge current density is neglected in this simple model. The surface charge gives rise to a bulk electric field inside the crystal along the polar axis $\boldsymbol{E}_B(t) = (\sigma(t)/\varepsilon\varepsilon_0)\boldsymbol{u}_z$. In turn, the bulk field incorporates a drift term to the current density with magnitude $\boldsymbol{j}_E = -\mu neE_B\boldsymbol{u}_z = -\mu ne\sigma/\varepsilon\varepsilon_0\,\boldsymbol{u}_z$, where μ and *n* are the electronic mobility and

the density of electronic carriers respectively. The time evolution of the accumulated surface charge density in the ± c surfaces is calculated integrating the equation $d\sigma = (j_{PV} + j_E)dt$ obtaining

$$\sigma_{\pm}(x,t) = \mp\sigma_{\infty}(x)[1-\exp(-t/\tau)] \tag{2}$$

where σ_∞ ($\sigma_\infty = \varepsilon\varepsilon_0 l_{PV} s I_0 D/\mu ne$) is the charge density accumulated at steady state at any of the surfaces, and $\tau = \varepsilon\varepsilon_0/\mu en = 1/\beta I$ is the time constant that is proportional to the inverse of the local intensity through $n = sID/\gamma A$ (A being the acceptor concentration of impurities [Fe^{3+}] and γ the electronic trapping coefficient). For more details on all these typical photorefractive relations and parameters see reference [20]. To have a first insight in the time dependence of σ it is useful to use a Taylor expansion:

$$\sigma(x,t) = \mp\sigma_{\infty}(x)\left[\beta I(x)t - \frac{1}{2}\beta^2 I^2(x)t^2 + \ldots\right] \tag{3}$$

It shows that $\sigma(x,t)$ is proportional to the light intensity and so, it is also sinusoidal if all terms excepting first order can be neglected, i.e. for short enough times. On the other hand, for very long times the space charge, as inferred from Eq. (2), become homogeneous ($\sigma(x,t) = \sigma_\infty$). However, it is worthwhile noting that possible transversal current contribution, neglected in this simple model, may affect particularly for long times near the steady state.

Hence, the charge redistribution generates: i) bulk PV fields $\boldsymbol{E}_B$ that can reach the same high values than in the parallel configuration, ii) the corresponding evanescent electric field outside the crystal nearby to the surface. The latter ones polarize the particles and attract them to the substrate via dielectrophoretic forces which for isotropic particles and in the Rayleigh approximation can be written as

$$\boldsymbol{F}_{DEP}(x,z,t) = \varepsilon_0 \alpha \nabla \boldsymbol{E}^2(x,z,t) \tag{4}$$

α being the particle polarizability [12]. Neutral particles should trap at the minima of the corresponding dielectrophoretic potential

$$V_{DEP}(x,z,t) = -\varepsilon_0 \alpha E_{out}^2(x,z,t) \tag{5}$$

We have numerically calculated the DEP potential corresponding to the surface charge distribution given by Eq. (2) for different light time exposures. To this end, we first calculate the evanescent electric fields $\boldsymbol{E}_{out}(x,z,t)$ by superposition of the coulomb contributions $d\boldsymbol{E}_{out}(x,z,t)$ associated to each elementary $dQ = \sigma dS$ along both crystal surfaces. Note, that the evanescent fields have both transversal, E_x, and vertical, E_z, components. From $\boldsymbol{E}_{out}(x,z,t)$ we trivially calculate $V_{DEP}(x,z,t)$ using Eq. (5).

In Fig. 2 we have represented the normalized surface charge density distribution $\sigma(x,t)$ and DEP potential on the surface for a sinusoidal illumination $I = I_0(1 + m\cos kx)$. $\sigma(x,t)$ is calculated using Eq. (2) and V_{DEP} as described in the previous paragraph. The light modulation m and light period $\Lambda = 2\pi/K$ have been chosen to be $m = 0.95$ and $\Lambda = 30$ μm, respectively. The sinusoidal intensity profile is also plotted for reference in Fig. 2(a).

It can be seen, that the surface charge, that is in phase with the light distribution, is sinusoidal only for the lowest time $t = 0.25\tau$, as already discussed through Eq. (3). For longer times the maxima markedly broaden, approaching a nearly flat profile for $t = 20\tau$. In turn, the DEP potential has pronounced minima coinciding with the regions of maximal charge accumulation and maximal light intensity. In this potential minima particle trapping should be possible and so, at difference with the parallel configuration [21], trapping occurs where light intensity is maximal. In addition the curve shape changes as t increases showing a narrower minima for intermediate times. Finally, for long enough times ($t \geq 20\tau$) in this simple model the dielectrophoretic potential is nearly flat and trapping progressively disappears. In summary, our simplified analysis on the DEP potential suggests that neutral particle patterning is indeed possible in this perpendicular configuration and that the illumination time plays an important role in the pattern morphology. Hence, in the rest of this work we will experimentally

investigate this perpendicular configuration that will be used for the first time for DEP trapping of neutral particles. Particular attention will be paid to 2D trapping in order to check whether the limitations of the parallel configuration are overcome.

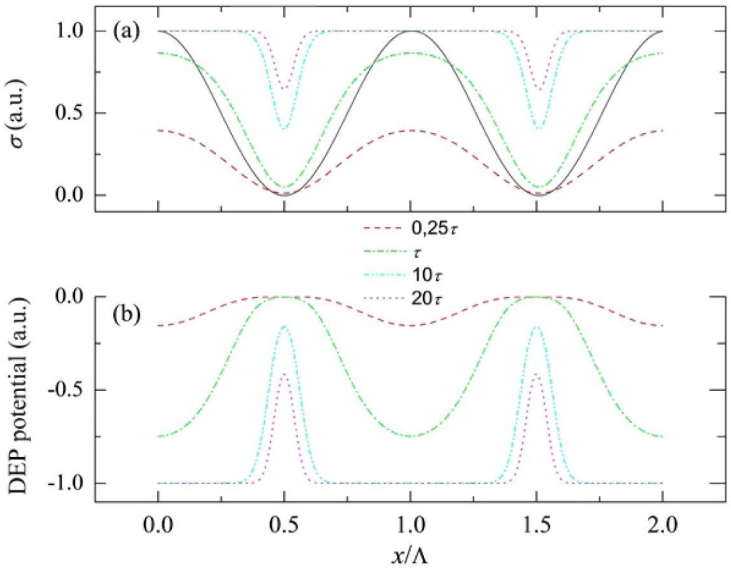

Fig. 2. Spatial distribution of (a) surface charge density and (b) dielectrophoretic potential in *z*-cut Fe:$LiNbO_3$ for sinusoidal illumination along the *x*-axis. Curves for light exposure times of 0.25τ, τ, 5τ, and 20τ are plotted. For reference, the illumination intensity profile is also drawn (solid line) in (a).

3. Experimental method and results

The experiments have been carried out in 1 mm thick *z*-cut congruent $LiNbO_3$ crystals highly doped with iron (~0.1% wt) in order to have a strong photovoltaic effect. For comparison, *x*-cut crystal samples with the same properties are also used.

We generate the particle patterns in a two-step process [18]: first, the substrate is illuminated to induce the PV fields. Second, after illumination, the substrate is immersed in a suspension of particles allowing them to deposit on the crystal surface. This sequential method simplifies the experiments and avoids the coupling of photovoltaic field trapping with pyroelectric effects [22] that might appear due to light-induced heating. Illumination has been carried out with a cw doubled Nd:YAG laser (λ = 532 nm) applying different 1D and 2D light patterns: sinusoidal patterns obtained by two-beam interference, rectangular homogeneous illumination using a rectangular slit and arbitrary 2D light patterns by image projection using a spatial light modulator (Holoeye LC–R1080 model).

After substrate illumination particle deposition is carried out using a non-polar hexane suspension (with null dipolar moment) in which the substrate is immersed during a time that we will call deposition time. The obtained particle patterns do not depend on the specific surface (+ *z* or –*z*) illuminated, as expected from dielectrophoretic trapping of neutral particles. Dielectric $CaCO_3$ micro-particles (diameter d~1–3 μm, homemade) and metallic aluminium nanoparticles (d~70 nm, bought to Skyspring Nanomaterials, Inc.) have been used. The neutrality of particles was also checked by simple electric experiments applying constant external DC fields to the hexane suspension observing no effect that could be associated to charged particles. The particle distribution was visualized by micro-photographs.

3.1 Singe-slit illumination experiments

A simple first experiment to check the viability of DEP trapping in the perpendicular configuration has been carried out illuminating the sample through a narrow slit, 2.1 mm wide. The situation corresponds essentially to the schematics of Fig. 1. After illumination, we deposited either micrometric $CaCO_3$ or nanometric Al particles from the hexane suspension. The same experiment but using a *x*-cut substrate (parallel configuration) is also performed for comparison. Photographs of the patterns obtained are presented in Fig. 3 for the perpendicular (Figs. 3(a) and 3(b)) and parallel (Figs. 3(c) and 3(d)) configurations. It is remarkable that successful DEP trapping of neutral particles has been obtained for the first time on a *z*-cut sample. Moreover, the results show significant differences between the perpendicular and the parallel configurations. In *x*-cut the particles trap at the two slit boundaries perpendicular to the polar axis independently of the sign of the bulk charges. This pattern, already found in previous work [13], is typical for dielectrophoretic trapping of neutral particles. In turn, for the perpendicular configuration they trap along the whole illuminated reproducing the light pattern. Note that in both geometries particles trap in the regions where bulk charges are accumulated (see Fig. 1) as it can be expected. Finally, it is worthwhile noting the ability of the configuration to trap either micrometric or nanometric particles.

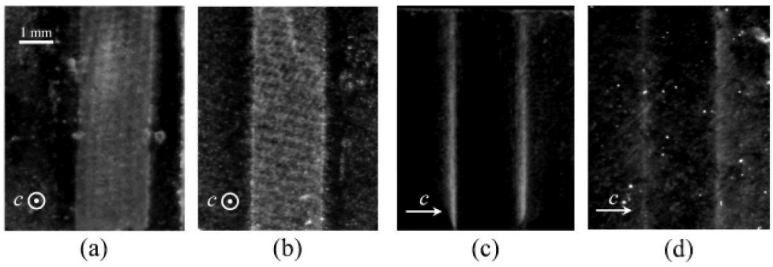

Fig. 3. Patterns obtained under homogeneous illumination through a rectangular slit for perpendicular, (a) and (b), and parallel geometries, (c) and (d), using $CaCO_3$ microparticles, (a) and (c), and aluminum nanoparticles, (b) and (d). In all case the light intensity on the substrate was 26 mW/cm^2.

3.2 Sinusoidal illumination

As a second step, we have checked the previously analyzed sinusoidal illumination, i.e. a light intensity pattern $I = I_0(1 + m\cos kx)$ with high contrast m. We have tested this illumination pattern with a *z*-cut configuration using a light period of 28 μm and $m = 0.95$, just the same parameters of simulation of Fig. 2. The light exposure time has been 10 min and the deposition time, i.e. the time of sample immersion in the particle suspension, 30 s. The result is shown in Fig. 4(a) where a well-defined periodic particle pattern with the same periodicity of light is clearly seen, as expected from theory. For comparison purposes a particle pattern obtained with an *x*-cut substrate with the same experimental conditions is shown in Fig. 4(b). The particle period is also the same of the light pattern. It is clearly seen that for sinusoidal light illumination and the experimental parameters used, the orientation of the crystal does not affect the main features of the pattern although perhaps the definition is slightly better in *x*-cut. Moreover, the period of the pattern ($\Lambda = 28$ μm) is remarkably low, not too far from the smallest value reported in the literature for *x*-cut which is about ~4 μm [18].

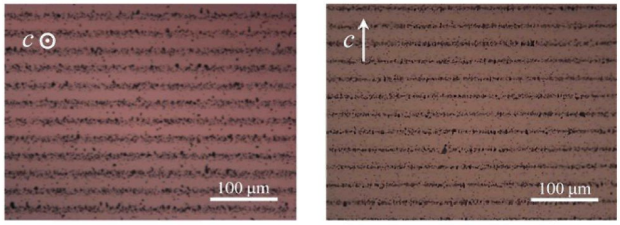

Fig. 4. Micro-photographs showing 1D periodic structuring of Al nanoparticles in (a) *z*-cut and (b) *x*-cut Fe:$LiNbO_3$. The particle period is 28 μm, $m = 0.95$ and the illumination light intensity 96 mW/cm^2.

We have also investigated the influence of the light time exposure in the deposited particle patterns that, according to theory, is a key parameter for *z*-cut. First, we have determined by a holographic technique [23] the time constant of the light–induced recording of the photovoltaic fields, resulting to be $\tau \approx 2$ min for the light intensity used in the experiment ($I_0 = I_1 + I_2 = 96$ mW/cm^2). We have carried out patterning experiments with the same experimental conditions of the previous experiments ($\Lambda = 28$ μm and $m = 0.95$) but for three different light exposure times of 30 s, 2 min. and 40 min. (i.e. 0.25τ, τ, 20τ). The particle deposition time is 30 s in all experiments. The results are shown in Fig. 5. Note that the experiment of Fig. 4(a) completes this series with its intermediate exposure time of 10 min (5τ) and to facilitate comparison it is also included in Fig. 5 as Fig. 5(c).

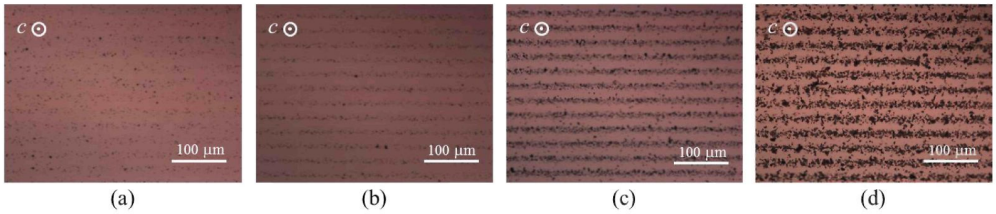

Fig. 5. Micro-photographs showing 1D periodic structuring of Al nanoparticles in *z*-cut Fe:$LiNbO_3$ for different light time exposures: (a) 0.25τ, (b) τ, (c) 5τ and (d) 20τ. The light intensity on the substrate was 96 mW/cm^2.

As it can be expected, the particle density increases with the time exposure obtaining a very well defined pattern for $t = 5\tau$ (Fig. 4(a)). On the other hand, the width of particle fringes is minimum for $t = \tau$ in rough agreement with theory. For long times ($t = 20\tau$) the particle pattern, although less clean than for shorter times, is still well defined having a width of fringes $d < \Lambda/2$ what is not in accordance with theoretical predictions (see Fig. 2). Then, as expected the simple model does not described well the results for long times. Anyhow, from a practical point of view, this is an advantageous result because particle patterning is also possible for long exposure times.

3.3 Two-dimensional patterns

Let us now investigate 2D patterning, the main objective of this work. To this end, a Fresnel lens type light distribution, obtained with the spatial light modulator, has been projected onto the sample. After illumination during 15 min., $CaCO_3$ particles have been deposited by a 20 s immersion in the hexane suspension. The obtained pattern is shown in Fig. 6(a) together with the corresponding pattern generated in a *x*-cut substrate (Figs. 6(b) and 6(c)) for comparison.

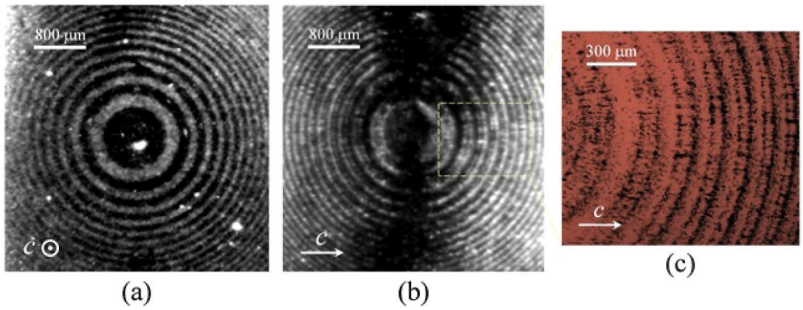

Fig. 6. Photographs of $CaCO_3$ microparticle patterns obtained from a Fresnel lens type light pattern on the surface of: (a) a *z*-cut substrate, and (b) a *x*-cut substrate. (c) Magnification of a region of the pattern (b) obtained with an optical microscope. Substrates were illuminated with a light intensity of 13 mW/cm^2.

The *z*-cut particle pattern exhibits a really good fidelity to the light pattern for any direction whereas the *x*-cut pattern is well defined for fringes perpendicular to the *z*-axis but disappears in the regions with fringes parallel to it. Moreover, in the microscopic image of a region of the *x*-cut pattern (Fig. 6(c)) it can be better appreciated that particles are placed at the boundaries of the illuminated rings analogously to the case of the single slit experiment (Fig. 3(c)). Then, as expected *z*-cut samples result to be much better templates for PV 2D neutral particle patterning accurately reproducing the light pattern.

In order to further investigate the 2D patterning capabilities at the nanometric scale we have also carried out experiments with metallic Al nanoparticles (d = 70 nm). We have used the same Fresnel lens pattern already applied with $CaCO_3$, and additionally, another one consisting in a mosaic of triangles. The results are shown in Fig. 7. It can be observed the good quality and definition of the patterns that accurately reproduce the light distribution, even in the vertex of triangles. They are even better defined than those obtained with $CaCO_3$, probably due to the smaller diameter of particles. On the other hand, it is also remarkable that large sizes (~5 × 5 mm) can be patterned with good quality and homogeneity, as it can be seen in Figs. 7(a) and 7(c).

4. Discussion and conclusions

The main throughput of this work is the demonstration that the so called perpendicular configuration (*z*-cut) of PV substrates allows efficient DEP trapping and patterning of neutral micro and nanoparticles. These results together with those obtained for 2D patterning of charged particles in reference [19] show clear advantages for operation of PV tweezers in this perpendicular configuration. Specifically, this configuration has two main properties, isotropic particle trapping over the crystal surface and local replica of the light pattern. These features are different from those of the parallel configuration (anisotropic particle trapping and contouring of the light regions) and imply a better performance especially for 2D patterning although are also useful for 1D.

The theoretical description of the generation of PV fields is not an easy task due to the nonlinear equations controlling PV transport [7,8]. The parallel configuration had been extensively studied in connection with photorefractive nonlinear optics [24]. Besides, very recent works of our group have analyzed it for PV trapping [12,21]. However, the analysis of the PV effect in the perpendicular configuration under inhomogeneous illumination had not been addressed so far, probably because it seemed not to be interesting for non-linear optical applications. Here, we have proposed a very simple preliminary model for the PV effect in *z*-cut Fe:$LiNbO_3$ and apply it for sinusoidal illumination. It predicts good capabilities of the perpendicular configuration for DEP patterning of neutral particles that have been corroborated by the experiments. The theory seems to reasonably describe the experiments for short and moderate exposure times but fails for long exposure times, very likely because the

transversal transport neglected in this simple model plays an important role for long times. Further work to accurately model this configuration should be very useful.

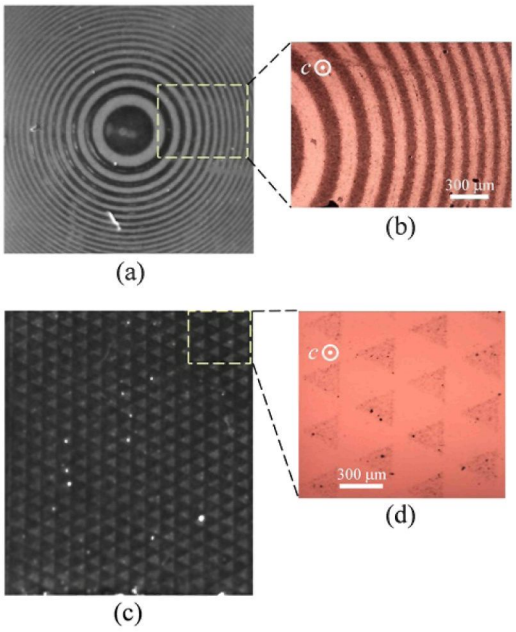

Fig. 7. Photographs of aluminum particles patterns on *z*-cut surfaces obtained using two different 2D light illuminations patterns (both with I = 13 mW/cm^2): (a) Fresnel lens type, and (c) mosaic of triangles; (b), (d) magnification of a region of the respective patterns obtained by optical microscopy.

Regarding experiments, it is remarkable that particle patterning has been obtained with all illumination patterns, demonstrating the unquestionable capability of this configuration to operate on neutral particles. It is worthwhile noting here that the main features of the particle patterns confirm the neutrality of the particles because they are only compatible with uncharged particles. Charged particles of one sign are not compatible with either the results for the single slit for *x*-cut of Figs. 3(c) and 3(d) (the patterns should be asymmetrical instead of symmetrical [13]) or the 2D results (at difference with our experiments, the particle pattern should appear in only one face of the crystal [19]). In turn, charged particles with two opposite signs are not compatible with results for sinusoidal illumination on *x*-cut substrates of Fig. 4(b) (the particle pattern could not have just the same period of light [19] as it is observed). On the other hand, the experiments using illumination through a slit are very simple but illustrative to remark the different behavior of the parallel and perpendicular configurations (see Fig. 3). As for sinusoidal illumination the results show similar capabilities to those of the parallel configuration. Moreover, remarkably low particle periods (30 µm) have been obtained not far from the smallest ones reported for the parallel configuration [18]. In fact, further reduction of the pattern periods is very likely reachable because optimization of this parameter has not been pursued in this first work.

Finally, for 2D illumination, the obtained particle patterns for the perpendicular configuration are really very good local replicas of the light images. The patterning is isotropic in the sense that it works for all directions at difference with the parallel configuration. Another important point is that large areas are patterned, what is often difficult to achieve with other methods such as conventional optical tweezers. Moreover, the local response to light illumination facilitates to design at will the particle patterns what is also difficult for other optoelectronic trapping approaches. In addition, one can expect the same

capabilities for pattern reconfiguration already demonstrated for the parallel configuration [14,16].

In summary, we can conclude that the perpendicular configuration is an outstanding advance in the development of PV tweezers assuring high quality 2D micro- and nanoparticle patterning and much simpler control of the trapping regions. This implies a remarkable progress that should convert PV tweezers in a very competitive tool among optoelectronic particle trapping techniques.

Acknowledgments

This work was supported by project MAT2011-28379-C03 and MAT2014-57704-C3.